PROCEEDINGS OF SPIE

SPIEDigitalLibrary.org/conference-proceedings-of-spie

FEM simulation of charging effect during SEM metrology

Duy Duc Nguyen, Jean-Herve Tortai, Mohamed Abaidi, Patrick Schiavone

Duy Duc Nguyen, Jean-Herve Tortai, Mohamed Abaidi, Patrick Schiavone, "FEM simulation of charging effect during SEM metrology," Proc. SPIE 10775, 34th European Mask and Lithography Conference, 107750P (19 September 2018); doi: 10.1117/12.2326609

SPIE.

Event: 34th European Mask and Lithography Conference, 2018, Grenoble, France

Downloaded From: https://www.spiedigitallibrary.org/conference-proceedings-of-spie on 30 May 2019 Terms of Use: https://www.spiedigitallibrary.org/terms-of-use

FEM simulation of charging effect during SEM metrology

Duy Duc Nguyen[a,b], Jean-Herve Tortai[b], Mohamed Abaidi[a], and Patrick Schiavone[a]

[a]ASELTA Nanographics, MINATEC-BHT 7, Parvis Louis Nel 38040, Grenoble cedex 9, France
[b]Univ. Grenoble Alpes, CNRS, CEA/LETI Minatec, LTM, F-38054 Grenoble Cedex, France

ABSTRACT

SEM metrology is widely used in microelectronics to control patterns dimensions after many processes, especially patterning. Process control is achieved by verifying that experimental dimensions match targeted ones. However SEM metrology may give erroneous measurements if strong charging occurs. Charging effect impacts on the SEM image contrast and introduces artefacts. This article intends to report on the modeling of the physical phenomena occurring when the electron gun scans a sample and how charging effect occurs. For this, charge dynamics are modeled by taking into account the drift kinetics and the diffusion of electrons. The corresponding Partial Differential Equation system is solved using FEniCS open software. First, we show that when only top view measurement are modeled, the typical contrast of SEM pictures can not be predicted. Second, cross section views are modeled. This time, the expected contrast behavior is obtained. Finally, a full 3D simulation is presented.

Keywords: Ebeam lithography, FEM, FEniCS, charging effect

1. INTRODUCTION

For technology nodes below 14nm, correction of proximity effects in E-beam maks lithography is mandatory to address the desired patterns that have high resolutions and high density. Aselta software (Inscale) allows generating a corrected layout that will compensate for these proximity effects. This is fulfilled by calibrating a compact model that predicts the final shape of the pattern. The optimum model is obtained by minimizing the error between the modeled shape and the experimental one that is measured by SEM. Conversely, any error in the SEM metrology will give inaccurate models. This is the major motivation for this work, nevertheless many other SEM imaging steps may benefit from a better modelling of the SEM imaging process.

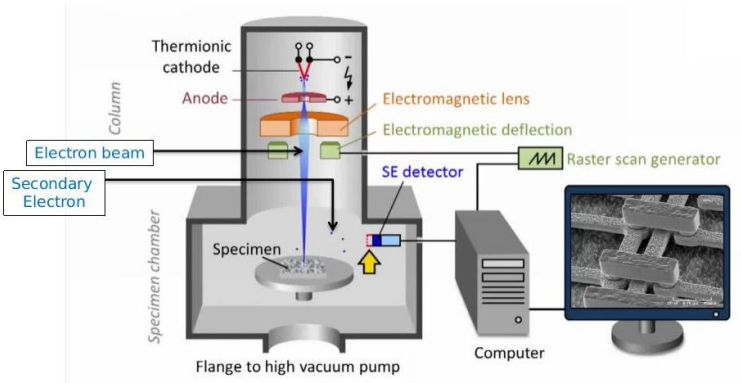

Figure 1: Sketch of how SEM image is created.

A scanning Electron Microscope (SEM) reconstructs the topography and material structure of a sample by scanning it with an electron gun and by collecting the electrons that are emitted by the sample surface. Finally, thanks to the synchronization of the scanning rate and the measured electrons, a gray scale picture is recorded

Further author information: (Send correspondence to Duy Duc Nguyen) E-mail: duy-duc.nguyen@aselta.com, Telephone: +33 (0) 7 52 91 85 16

34th European Mask and Lithography Conference, edited by Uwe F.W. Behringer, Jo Finders, Proc. of SPIE Vol. 10775, 107750P · © 2018 SPIE
CCC code: 0277-786X/18/$18 · doi: 10.1117/12.2326609

Downloaded From: https://www.spiedigitallibrary.org/conference-proceedings-of-spie on 30 May 2019
Terms of Use: https://www.spiedigitallibrary.org/terms-of-use

pixel per pixel. The brightness of each pixel is proportional to the number of electrons that are detected when the sample is scanned. Figure 1* illustrates SEM principles. As long as the sample is hit with the electron gun, electrons penetrate the material and lose their energy due to successive random collisions with atoms. Some electrons are back scattered from the volume, others are scattered at the sample surface due to the topography and finally some low energy electrons are entrapped.[1] Secondary electrons or back scattered electrons are those collected by the SEM detectors. The physic of interaction between electrons and atoms is stochastic and is well predicted using Monte Carlo softwares (CASINO,[2] CHARIOT,[3] JMONSEL[4]).

The charging of the sample occurs when the specimen has an excess or a lack of electrons. It impacts SEM images by modifying the number of electrons that are collected by the detectors.[5] Precisely, there are two kinds of charging; negative charging occurs when electrons are entrapped in the specimen while positive charging appears when the number of the electrons exiting from the specimen is larger than that flowing to the specimen. Charging effect is caused by the fact that secondary electron trajectory is influenced by negative or positive charges excess. If the specimen is negatively charged more secondary electrons enter the detector, leading to a greyscale value of the pixel shifted to bright value. Whereas, if the specimen is positively charged, less secondary electrons enter the detector, so that the locally charged area induces a darker pixel. For example, Figure 2 † shows an affected SEM image with negative charging leading to anomalous black tails following patterns.

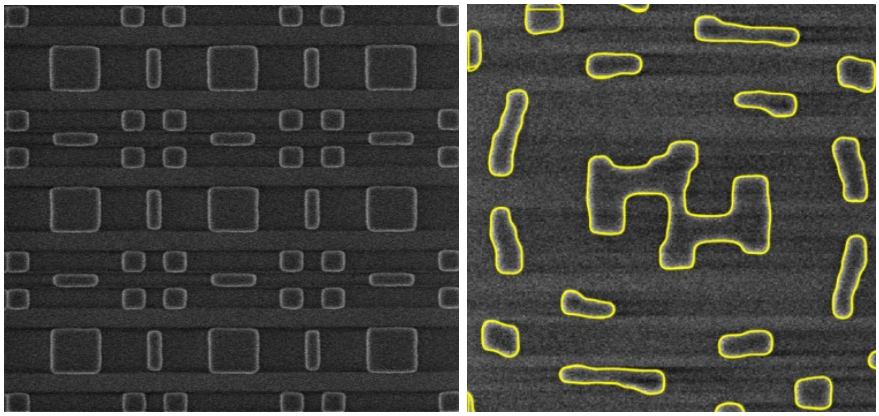

Figure 2: Affected SEM image with anomalous tailing.

2. THEORETICAL BACKGROUND

Charging can significantly impact CD-SEM metrology. In order to remove this influence, we have to understand how the charges and the potential behave under the incident electron beam on the sample with various surface topologies and materials. The classical drift-diffusion model is a good candidate because it shows fundamental semiconductor physics such as the motion, generation and recombination of charges in relation with the electric field. The drift-diffusion model is a system of Partial Differential Equations (PDEs) containing the diffusion and drift terms. The diffusion term points out the net movement of charges from a region of high concentration to a region of low concentration and it is described mathematically as the divergence of gradient of the charges. The drift term shows the transport of charges within electric field and it is described mathematically as the divergence of the charges multiplied with the velocity field and is similar to a fluids motion. Moreover, to represent the dynamic evolution of charges over time, their rate of change are added into the drift-diffusion equations. As charges are generated, the potential changes and diffuses. In turn, the electric field created by the potential affects the flow of the charges. Solving such PDEs system necessitates postulating for initial conditions and boundary conditions. We assume that there are no charges at some edges depending on the geometry of the

*The picture is taken from published lecture of Karlsruhe University of Applied Sciences, Germany.

†The picture is taken from.[5]

Downloaded From: https://www.spiedigitallibrary.org/conference-proceedings-of-spie on 30 May 2019
Terms of Use: https://www.spiedigitallibrary.org/terms-of-use

sample and there is intrinsic concentration of charges at the beginning of time. The model is given as follows

$$\begin{cases} \varepsilon_0 \varepsilon \nabla \cdot \boldsymbol{E} = q_e \left(p - n\right) & \text{in} \quad \Omega \times (0, t_{end}] \\ \dfrac{\partial n}{\partial t} = \dfrac{1}{q_e} \nabla \cdot \boldsymbol{J}_n + S_n - R & \text{in} \quad \Omega \times (0, t_{end}] \\ \dfrac{\partial p}{\partial t} = -\dfrac{1}{q_e} \nabla \cdot \boldsymbol{J}_p + S_p - R & \text{in} \quad \Omega \times (0, t_{end}] \end{cases} \tag{1}$$

$$\text{with } \boldsymbol{J}_n = q_e \left(\mu_n n \boldsymbol{E} + D_n \nabla n\right), \ \boldsymbol{J}_p = q_e \left(\mu_p p \boldsymbol{E} - D_p \nabla p\right),$$

$$\text{and } \varphi = p = n = 0 \text{ on } \Gamma_D, \nabla \varphi \cdot \boldsymbol{\eta} = \nabla p \cdot \boldsymbol{\eta} = \nabla n \cdot \boldsymbol{\eta} = 0 \text{ on } \Gamma_N \text{ and } \varphi = 0, n = n_i, p = p_i \text{at} t = 0,$$

where Ω denotes a given scanned surface or volume, Figures 3, 4, 5, $\partial\Omega$ denotes the boundary of Ω, Γ_D and Γ_N denotes portions of $\partial\Omega$ where Dirichlet and Neumann boundary conditions are applied, $t \in (0, t_{end}]$ denotes time variable and time interval, $p\left(\boldsymbol{x}, t\right)$ and $n\left(\boldsymbol{x}, t\right)$ denote hole and electron densities, D_n and D_p denote electron and hole diffusion coefficients, μ_n and μ_p denote electron and hole drift mobilities, $\boldsymbol{J}_n\left(\boldsymbol{x}, t\right)$ and $\boldsymbol{J}_p\left(\boldsymbol{x}, t\right)$ denote electron and hole currents respectively. The notation $\boldsymbol{E} = -\nabla\varphi$ denotes electric field with $\varphi\left(\boldsymbol{x}, t\right)$ is potential, ε_0 denotes absolute permittivity of the vacuum, ε denotes relative permittivity and q_e denotes elementary charge. The notation $S_n\left(\boldsymbol{x}, t\right)$ and $S_p\left(\boldsymbol{x}, t\right)$ are the source terms which is expressed in a Point Spread Function (PSF)[67] . For the sake of simplicity, we assumed S_p is smaller than S_n by being a fraction of it, precisely,

$$S_n(n,p) = \frac{I_0}{q_e(2\pi)^{3/2}\sigma_x\sigma_y\sigma_z} exp\left(-\left(\frac{(x-Bx)^2}{\sigma_x^2} + \frac{(y-By)^2}{\sigma_y^2} + \frac{(z-Bz)^2}{\sigma_z^2}\right)\right), S_p(n,p) = 10^{-5} S_n, \tag{2}$$

where Bx, By, Bz are coordinates of the electron gun which are updated according to the scanning speed, $\sigma_x, \sigma_y, \sigma_z$ are width, length and depth (electron range) of the electron interaction volume, I_0 is incident electron current, r_i is spot size. Once electrons are entrapped in the sample, a rapid recombination term appears that tends to compensate for this electron excess so electro-neutrality is maintained shortly. In our implementation, this recombination term, denoted $R\left(\boldsymbol{x}, t\right)$ follows the Shockley-Read-Hall model formulated as

$$R(n,p) = \frac{np - n_i^2}{\tau_p(n+n_1) + \tau_n(p+p_1)}, n_1 = N_c exp\left(\frac{E_t - E_c}{kT}\right), p_1 = N_v exp\left(\frac{E_v - E_t}{kT}\right) \tag{3}$$

where n_i denotes intrinsic carrier concentration, τ_n and τ_p denote electron and hole average lifetime, N_v and N_c denote effective density of states according to valence and conductor bands, k denotes Boltzmann constant and T denotes temperature.

3. MODELING STRATEGY

The analytical solution of the PDEs (1) generally can not be found for the vast majority of geometries. Instead, an approximation of the PDEs (1) is constructed by discretization methods. The Finite Element Method (FEM) is our choice. We have chosen FEniCS to be our simulation tool which is a well-known open-source computing platform for quickly translating scientific models into efficient finite element code. To start the numerical method process, the PDEs (1) is transferred into a simplified form called weak formulation that enables using the concepts of linear algebra to solve the problem. In the weak formulation, PDEs (1) do not need to hold absolutely and have instead weak solutions only with respect to certain "test function". The appropriate space for test function is given by $W^1_{\Gamma_0}(\Omega) = H^1_{\Gamma_D}(\Omega) \times H^1_{\Gamma_D}(\Omega) \times H^1_{\Gamma_D}(\Omega)$ where

$$H^1(\Omega) = \{v \in L^2(\Omega) \mid ||v||_{L^2(\Omega)} + ||\nabla v||_{L^2(\Omega)} < \infty\}, H^1_{\Gamma_D}(\Omega) = \{v \in H^1(\Omega) \mid v = 0 \text{ on } \Gamma_D\}.$$

Multiplying the system (1) with any test function $(\overline{\varphi}, \overline{n}, \overline{p}) \in W^1_{\Gamma_D}(\Omega)$, integrating it over the domain Ω and applying integration by parts with $\overline{\varphi}, \overline{n}$ and applying boundary conditions, we get three equations as follows

$$\varepsilon_0\varepsilon \int_\Omega \nabla\varphi\nabla\overline{\varphi} \ \mathrm{d}x = q_e \int_\Omega (p-n)\,\overline{\varphi} \ \mathrm{d}x, \int_\Omega \frac{\partial n}{\partial t}\overline{n} \ \mathrm{d}x = -\frac{1}{q_e}\int_\Omega \boldsymbol{J}_n \cdot \nabla\overline{n} \ \mathrm{d}x + \int_\Omega (S_n - R) \ \mathrm{d}x \text{ and}$$

Downloaded From: https://www.spiedigitallibrary.org/conference-proceedings-of-spie on 30 May 2019
Terms of Use: https://www.spiedigitallibrary.org/terms-of-use

$$\int_\Omega \frac{\partial p}{\partial t}\overline{p}\ \mathrm{d}x = \frac{1}{q_e}\int_\Omega \boldsymbol{J}_p \cdot \nabla \overline{p}\ \mathrm{d}x - \int_\Omega (S_p - R)\ \mathrm{d}x.$$

By summing these equations, we get

$$\begin{aligned} res := \varepsilon_0 \varepsilon \int_\Omega \nabla\varphi \cdot \nabla\overline{\varphi}\ \mathrm{d}x - q_e \int_\Omega (p-n)\,\overline{\varphi}\ \mathrm{d}x + \int_\Omega \frac{\partial n}{\partial t}\overline{n}\ \mathrm{d}x + \frac{1}{q_e}\int_\Omega \boldsymbol{J}_n \cdot \nabla\overline{n}\ \mathrm{d}x \\ - \int_\Omega (S_n - R)\,\overline{n}\ \mathrm{d}x + \int_\Omega \frac{\partial p}{\partial t}\overline{p}\ \mathrm{d}x - \frac{1}{q_e}\int_\Omega \boldsymbol{J}_p \cdot \nabla\overline{p}\ \mathrm{d}x + \int_\Omega (S_p - R)\overline{p}\ \mathrm{d}x = 0 \end{aligned} \tag{4}$$

The week problem is stated as finding $(\varphi, n, p) \in W^1_{\Gamma_D}(\Omega)$ such that (4) satisfies for all $(\overline{\varphi}, \overline{n}, \overline{p}) \in W^1_{\Gamma_D}(\Omega)$. Besides, we use backward Euler (or implicit Euler) as our time discretization scheme such as

$$\frac{\partial u}{\partial t}(t_{i+1}) \simeq \frac{u(t_{i+1}) - u(t_i)}{dt},$$

where $t_i = i * dt \in (0, t_{end}]$, dt is time step defined by $dt = t_{end}/|\{i\}|$ and u being n or p. In addition, Finite Elements necessitates a mesh that will define elementary sub-domains. Computation time is strongly related to the number of sub domains, the best compromise being adaptive mesh were resolution is increased where it is needed while large mesh can be used where smooth parameter variation occurs. In our case, the adaptive mesh is created by an open software called GMSH. Using adaptive mesh reduces the computation time enormously. Typically, the fine mesh is set only in the neighborhood of the excitation beam instead of everywhere in the domain. For instance, the mesh has $2[nm]$ diameter in the area that covers the beam width and depth and has $10[nm]$ in the remaining area. In order to be able to generate an image-like simulation, we implemented the scanning mode of solution. The incident beam S_n goes from the left to the right at the middle of the domain. Besides, it stays $t_{spot} = 50\,[ns]$ at each pixel of $4\,[nm^2]$. In the two dimensional space, we introduce top and cross section simulations which allow us to observe the distribution of the electron and the potential in x, y or z directions. In three dimensional space, we introduce simulations similar to ones in two dimensional space. In the examples given in this paper, the specimen is made of Silicon (Si) and the pattern is made of Silicon dioxide (SiO2).

XY-Simulation The domain Ω is defined as a rectangle of $250 \times 200[nm^2]$ having a pattern of $50 \times 100[nm^2]$ located in the center of the domain. The boundaries Γ_D is the top and the bottom boundaries and Γ_N is the left and right boundaries, Figure 3.

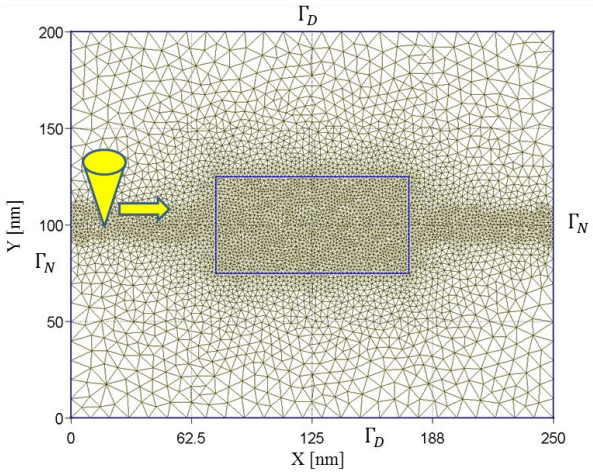

Figure 3: Plot of geometry and mesh designed by GMSH for XY-simulation.

XZ-Simulation The domain Ω is defined as a rectangle of $250 \times 50[nm^2]$ having a pattern of $40 \times 100[nm^2]$ located in the middle of the top surface. The pattern has a slope of $5[nm]$ on each sides. The boundaries Γ_D is the bottom boundary and Γ_N is the left and right boundaries, Figure 4.

Downloaded From: https://www.spiedigitallibrary.org/conference-proceedings-of-spie on 30 May 2019
Terms of Use: https://www.spiedigitallibrary.org/terms-of-use

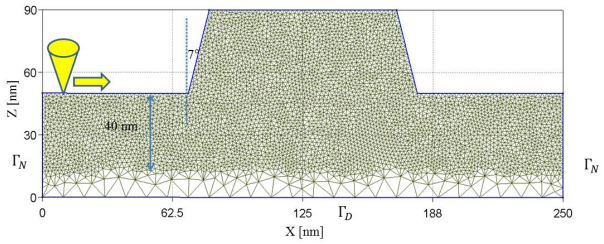

Figure 4: Plot of geometry and mesh designed by GMSH for XZ-simulation.

3D-Simulation The domain Ω is defined as a rectangle of $250 \times 200 \times 50[nm^3]$ having a pattern of $100 \times 50 \times 40[nm^3]$ located in the center of the top surface. The boundaries Γ_D is the bottom boundary and Γ_N is the lateral boundaries, Figure 5.

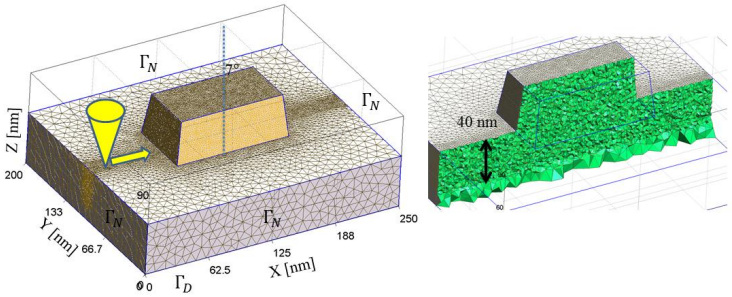

Figure 5: Plot of geometry and mesh designed by GMSH for 3D simulation.

In the case of XZ and 3D simulations, the sources are implemented close to the upper surface. Its x and y coordinates are increased linearly according to the increment of time while its z-coordinate is computed according to the z-coordinates of mesh nodes of the surface that surround the beam location. The distribution of the sources will vary due to the variety of the surface geometry, for example see Figure 6.

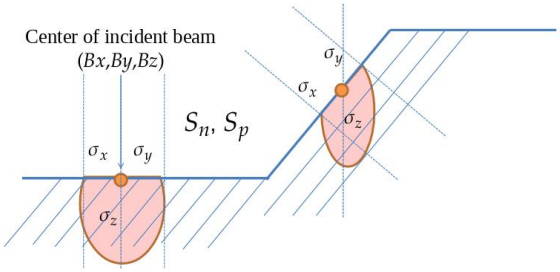

Figure 6: Plot of sources implementation and variety.

Besides, we assumed $\sigma_x = \sigma_y = 7[nm]$ when the incident beam hits Si or SiO_2 material with a normal incidence and $\sigma_z = 10$ and $15[nm]$ when it hits Si and SiO_2 materials respectively. These values are obtained from Monte Carlo simulations of electron scattering at 1keV entering the Si, SiO_2 specimens with 90^0 and 83^0 angles respectively. The first angle corresponds to the case of the beam inpinging on a flat surface while the second one is relative to the sloped edge of the pattern surface, as illustrated Figure 7.

4. RESULTS

The FEniCS software is asked to solve (4) at each dt and store results into matrices containing the position of each mesh nodes and corresponding values, i.e. n, p or φ. These results are then plotted by an open software called Paraview. For examples, a few results of computation of n repartition at different steps of the scan mode

Downloaded From: https://www.spiedigitallibrary.org/conference-proceedings-of-spie on 30 May 2019
Terms of Use: https://www.spiedigitallibrary.org/terms-of-use

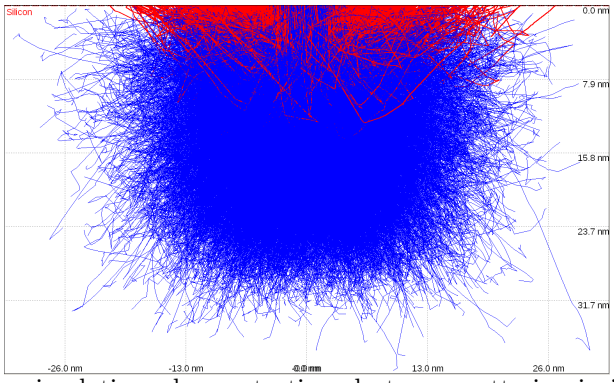

Figure 7: Plot of Monte Carlo simulations demonstrating electrons scattering inside Si specimen; where 20000 electrons are lunched with 1KeV energy. The incident beam comes at 90^0 angle. From CASINO Software

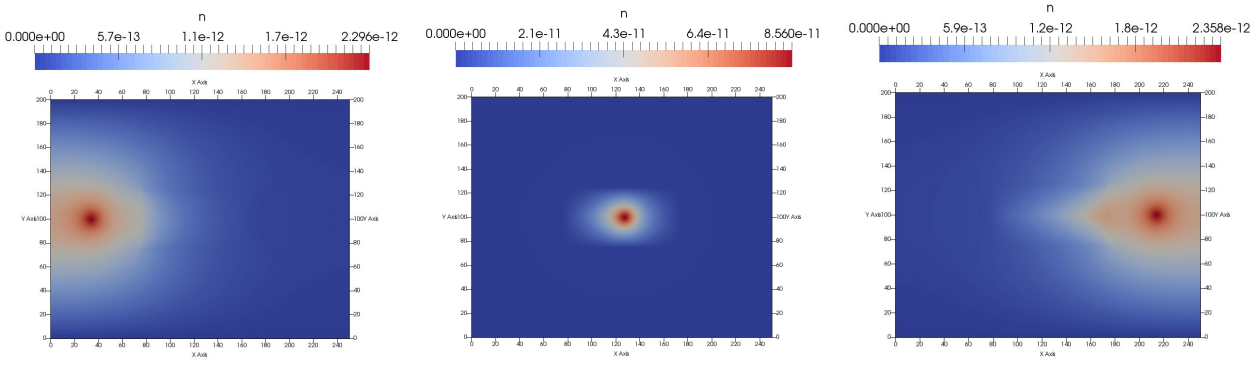

Figure 8: Plot of n according to different locations of S_n of XY simulation (Top View).

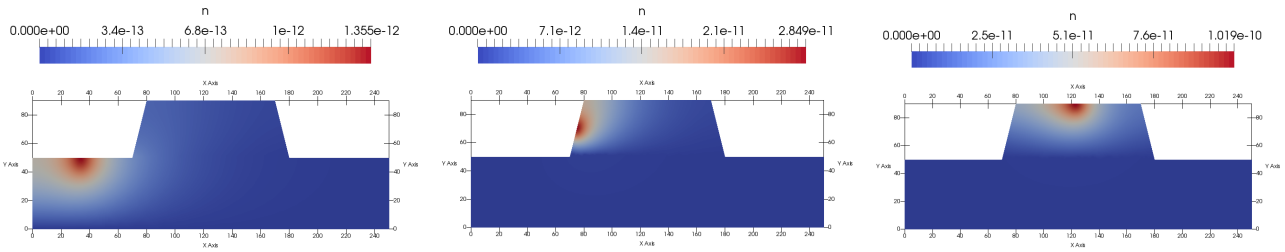

Figure 9: Plot of n according to different locations of S_n of XZ simulation (Cross Section).

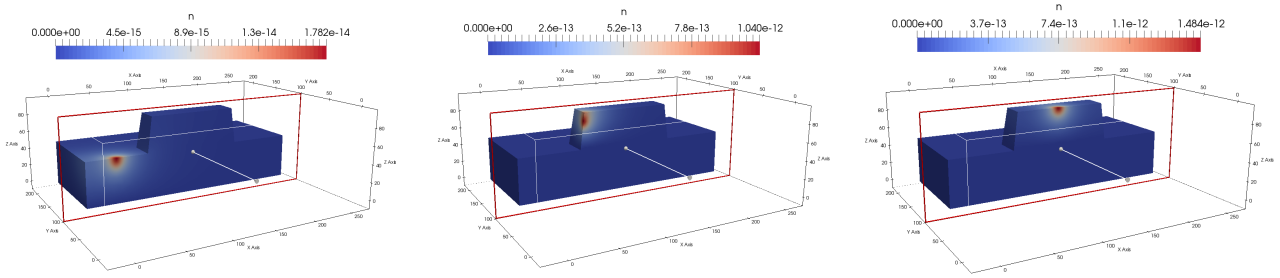

Figure 10: Plot of n according to different locations of S_n of 3D simulation.

Downloaded From: https://www.spiedigitallibrary.org/conference-proceedings-of-spie on 30 May 2019
Terms of Use: https://www.spiedigitallibrary.org/terms-of-use

are plotted in Figures 8, 9, 10. These figures show that the electron, and hole concentration as well as the potential are much higher in SiO_2 pattern than in the Si substrate which indicates that with no surprise the charging effect occurs mainly in the SiO_2 pattern. Then, we plot $max_t(n)$ in Figures 11 which shows that the electron concentration reaches maximum at the edges of SiO_2 pattern. It explains why there are two peaks on the typical SEM images, Figure 11b, 11c. The Figure 11a shows that XZ-Simulation loses topological effect.

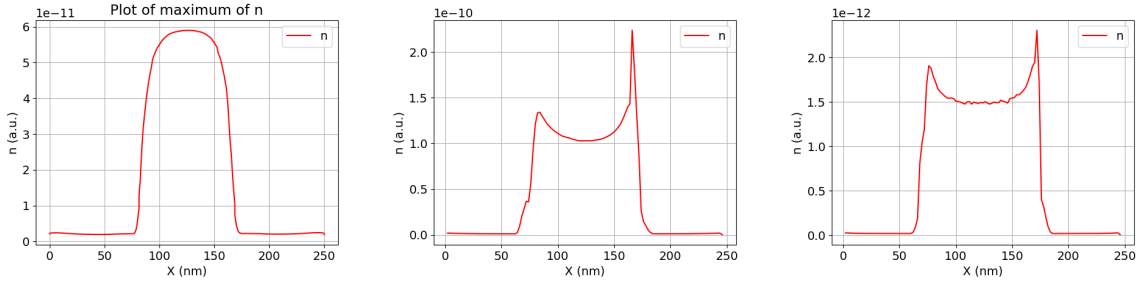

(a) XY-Simulation (b) XZ-Simulation (c) 3D-Simulation

Figure 11: Plot of $max_t(n)$.

5. CONCLUSION AND PERSPECTIVE

The main physical phenomena such as distribution of electron, hole and potential resulting during electron beam imaging of Silicon dioxide patterns over a Silicon substrate have been studied. The model implementation shows that FEniCS has a great potential for our needs. The concentration of electron, hole and potential have been computed and plotted. Adaptive meshes have been created by GMSH resulting in a very significant reduction of simulation runtime. Finally, we mention continued works. To simulate more realistic problem and improve accuracy we will implement jump boundary condition between dioxide and semiconductor as the flow of charge should be continuous. We plan to bring other numerical improvements such as parallelization ans mesh size optimization. The major step though will be to emulate the detection stage that actually produces the real SEM image.

REFERENCES

[1] Cazaux, J., "Charging in scanning electron microscopy from inside and outside," *Scanning* **26**(4), 181–203 (2004).

[2] Drouin, D., Couture, A. R., Joly, D., Tastet, X., Aimez, V., and Gauvin, R., "Casino v2. 42a fast and easy-to-use modeling tool for scanning electron microscopy and microanalysis users," *Scanning* **29**(3), 92–101 (2007).

[3] Babin, S., Borisov, S., Ivanchikov, A., and Ruzavin, I., "Chariot: software tool for modeling sem signal and e-beam lithography," *Physics Procedia* **1**(1), 305–313 (2008).

[4] Villarrubia, J. S., Vladár, A., Ming, B., Kline, R. J., Sunday, D. F., Chawla, J., and List, S., "Scanning electron microscope measurement of width and shape of 10nm patterned lines using a jmonsel-modeled library," *Ultramicroscopy* **154**, 15–28 (2015).

[5] "Scanning Electron Microscope A to Z (SEM): Basic knowledge for using the SEM." https://www.jeol.co.jp/en/applications/pdf/sm/sem_atoz_all.pdf.

[6] Alles, B., Cotte, E., Simeon, B., and Wandel, T., "Modeling the work piece charging during e-beam lithography," in [*SPIE Advanced Lithography*], 69244P–69244P, International Society for Optics and Photonics (2008).

[7] Maslovskaya, A. and Pavelchuk, A., "Simulation of dynamic charging processes in ferroelectrics irradiated with sem," **476**(1), 1–11 (2015).

Downloaded From: https://www.spiedigitallibrary.org/conference-proceedings-of-spie on 30 May 2019
Terms of Use: https://www.spiedigitallibrary.org/terms-of-use